2010-01-01

Visible Near-Infrared Hyperspectral Imaging for the Identification and Discrimination of Brown Blotch Disease on Mushroom (Agaricus bisporus) Caps

Edurne Gaston
Technological University Dublin, edurne.gaston@tudublin.ie

Jesus Maria Frias
Technological University Dublin, Jesus.Frias@tudublin.ie

Patrick Cullen
Technological University Dublin, pjcullen@tudublin.ie

Colm O'Donnell
University College Dublin

Aoife Gowen
University College Dublin, aoife.gowen@ucd.ie

Recommended Citation

, Frias JM. et al. (2010) Visible-near infrared hyperspectral imaging for the identification and discrimination of brown blotch disease on mushroom (Agaricus bisporus) caps. Journal of Near Infrared Spectroscopy Volume 18 Issue 5, Pages 341–353. doi.org/10.1255/jnirs.894

Visible Near-Infrared Hyperspectral Imaging for the Identification and Discrimination of Brown Blotch Disease on Mushroom (*Agaricus bisporus*) Caps

EDURNE GASTON[1], JESÚS M. FRÍAS[1*], PATRICK J. CULLEN[1], COLM P. O'DONNELL[2] and AOIFE A. GOWEN[2].

[1]School of Food Science and Environmental Health, Dublin Institute of Technology, Cathal Brugha Street, Dublin 1, Ireland.

[2]Biosystems Engineering, School of Agriculture, Food Science and Veterinary Medicine, University College Dublin, Dublin 4, Ireland.

*Corresponding author. E-mail: Jesus.Frias@dit.ie

Abstract

Brown blotch, caused by pathogenic *Pseudomonas tolaasii* (*P. tolaasii*), is the most problematic bacterial disease in *Agaricus bisporus* mushrooms. Although it does not cause any health problems, it reduces the consumer appeal of mushrooms in the market place, generating important economical losses worldwide. Hyperspectral imaging (HSI) is a non-destructive technique that combines imaging and spectroscopy to obtain information from a sample. The objective of this study was to investigate the use of HSI for brown blotch identification and discrimination from mechanical damage on mushrooms. Hyperspectral images of mushrooms subjected to i) no treatment, ii) mechanical damage or iii) microbiological spoilage were taken during storage and spectra representing each of the classes were selected. Partial least squares- discriminant analysis (PLS-DA) was carried out in two steps: i) discrimination between undamaged and damaged mushrooms and ii) discrimination between damage sources (i.e. mechanical or microbiological). The models were applied at a pixel level and a decision tree was used to classify mushrooms into one of the aforementioned classes. A correct classification of >95% was achieved. Results from this study could be used for the development of a sensor to detect and classify mushroom damage of mechanical and microbial origin, which would facilitate the industry to make rapid and automated decisions to discard produce of poor marketability.

Keywords: mushrooms, *Agaricus bisporus*, brown blotch, *Pseudomonas tolaasii*, mechanical damage, vis-NIR hyperspectral imaging, PLS-DA.

Introduction

Cultivated mushrooms are susceptible to a variety of pests and diseases. *Pseudomonas tolaasii* (*P. tolaasii*) is the causal agent of brown blotch (also known as bacterial blotch) disease[1] and the most important pathogenic bacterium of *Agaricus bisporus*[2]. This disease has been detected and described worldwide and affects not only the button mushroom market but the mushroom market in general[3]. According to growers, brown blotch is "the worst disease", because of the large economic losses associated to it. Brown blotch can cause a general loss of crop yield of 10 % and a decrease in quality of another 10 %[4]. The most typical symptoms of brown blotch are pitting and browning of mushroom tissues, induced by the watersoluble toxin tolaasin[5]. This extracellular toxin is produced by the pathogenic form of *P. tolaasii*[6]. The colonisation of mushroom caps by *P. tolaasii* results in the appearance of unappealing brown spots on the mushroom cap and stipe[3]. Lesions are slightly concave blemishes, sometimes small, round or spreading in many directions[7]. When the damage is more intense, the spots are darker and sunken. Browning affects only the external layers of the cap tissue and is restricted to 2-3 mm below the surface of the cap.

The mushroom industry is in need of objective evaluation methodologies to ensure that only high quality produce reaches the market[8]. Studies in the field of brown blotch detection include the work of Vízhányó and Felföldi[9], who tested the potential of a machine vision system to recognise and identify brown blotch and ginger blotch diseases, both of which cause discolouration in mushroom caps. A vectorial normalisation method was developed to decrease the effect of the natural loss of whiteness of the mushroom surface and increase the differences in the image caused by the disease. The method showed an ability to discriminate between discolouration caused by microbial disease and other sources of discolouration, such as natural senescence. However, no attempt was made to discriminate brown blotch from

bruises induced by mechanical stress, which is also an important source of discolouration and quality loss in the mushroom industry[10].

Hyperspectral imaging (HSI) is a rapid and non-destructive technology that has recently emerged as a powerful alternative to conventional imaging for food analysis[11]. Hyperspectral images are composed of hundreds of contiguous wavebands for each spatial position of an object. Consequently, each pixel in a hyperspectral image contains the spectrum of that specific position. Hyperspectral images, known as *hypercubes*, are three-dimensional blocks of data, comprising two spatial and one wavelength dimension. The large quantities of highly correlated data contained in a hypercube are well suited to analysis by dimension reduction approaches such as principal components analysis (PCA) and partial least squares-discriminant analysis (PLS-DA)[12]. PLS-DA can also be applied to develop qualitative models for supervised classification between various sample classes.

HSI has been applied at various levels in the assessment of safety and quality of food, including constituent analysis[13-15], quality evaluation[16, 17] and detection of contaminants[18, 19] and defects[20]. Additionally, a number of researchers have reported the potential of HSI for identification of microorganisms of concern in food[21, 22]. In the field of mushrooms, HSI has proved useful for the detection of bruise[23] and freeze[24] damage and the prediction of moisture content[25] and enzyme activity[26], as well as for the evaluation of shelf-life[27] and quality deterioration[28]. Recent advances in the detection of skin damage of other products include work by Ariana et al.[29] with cucumbers and Nicolaï et al.[30] and ElMasry et al.[31] with apples. As regards damage of microbial origin, Gómez-Sanchis et al.[32] proposed a hyperspectral imaging system for the early detection of rot caused by *Penicillium digitatum* (fungi) in mandarins. This method's success in classifying rotten fruit was above 91% and it represented an alternative to the operationally inefficient sorting system previously used in the citrus industry. While evidence from the literature points to its feasibility, to the authors'

knowledge, HSI has not been used to detect damage of bacterial origin in horticultural products.

The objective of this study was to investigate the potential application of Vis-NIR HSI for brown blotch identification on mushroom caps and for its discrimination from mechanical damage injuries.

Materials and methods

Mushroom supply and damage

Agaricus bisporus mushrooms (strain Sylvan A15, Sylvan Spawn Ltd., Peterbourough, UK) were grown in plastic bags and tunnels in Kinsealy Teagasc Research Centre (Kinsealy, Co. Dublin, Ireland) following common practice in the mushroom industry. Only uniform undamaged closed cap mushrooms from the 1st and 2nd flush with a diameter of 3-5 cm were hand-picked in November 2008 (training set) and July 2009 (test set). Samples were placed in a metal grid and carefully delivered to the laboratory in purpose-built containers, to minimise mechanical damage during transport**.** Mushrooms arrived at the laboratory premises within 1 hour after harvesting and were stored overnight at 4°C.

For each set of mushrooms (n_{train} = 144 and n_{test} = 108), samples were divided in 3 groups (undamaged (U), mechanically damaged (MD) and *P. tolaasii* inoculated mushroom (PT)) of equal size ($n_{train,i}$ = 48 and $n_{test,i}$ = 36, where i = U, MD, PT).

Each mushroom class was treated as follows:

U: No treatment.

MD: samples were subjected to vibrational bruising to simulate crop handling and transport. Mushrooms were damaged in batches of 600g (approx) units inside polystyrene plastic boxes. Mechanical damage was induced by using a Gyratory Shaker Model G2

shaking table (New Brunswick scientific Co., Edison, N.J., USA) at 300 rpm amplitude for a shaking period of 10 min. Samples were stored in an environmental incubator (MLR-350 HT, SANYO Electric Biomedical Co. Ltd., Japan) at 25°C and 90 % relative humidity (RH) for 24 h prior to imaging.

PT: samples were obtained by inoculating 4 drops of 10 µL/each of a solution of pathogenic *P. tolaasii* onto each clean cap at 4×10^6 cfu. Samples were stored in the incubator for 48 h at 25°C and 90 % RH prior to imaging, to encourage appearance of brown blotch symptoms on the mushroom caps.

A total number of 252 mushrooms were used in this experiment.

Pathogenic *P. tolaasii* solution

Freeze-dried culture (DMS no. 19342) was purchased from Deutsche Sammlung von Mikroorganismen und Zellkulturen GmbH (DSMZ), Germany, resuspended in nutrient broth (NB, Scharlau, Dublin) and incubated at 25°C for 24 h. The pure culture was transferred into nutrient agar plates (NA, Oxoid, Dublin) and incubated at optimal conditions to obtain isolated colonies.

"Mushroom tissue block rapid pitting" and "White Line in Agar" (WLA) pathogenicity tests were carried out following the procedure of Wong and Preece[33] to confirm culture pathogenicity on mushrooms.

- *Mushroom tissue block rapid pitting test*

The outer skin of a mushroom was peeled off and mushroom cap tissue blocks of approx. 15 × 15 × 5 mm were cut. Bacterial isolates were grown on Pseudomonas agar base (PAB, Oxoid, Dublin) at 25°C for 24 h and suspended in sterile distilled water (10^8 cfu mL^{-1} approx). Mushroom blocks were placed in duplicate on Petri dishes containing sterile water-moistened filter paper. The bacterial solution was inoculated onto the cut

surface of one of the mushroom blocks and incubated at 25°C. Sterile water was inoculated onto the surface of the other mushroom blocks for negative control. Pitting of the cut surface of mushroom tissue revealed pathogenicity of *P. tolaasii* on the mushroom blocks.

"White Line in Agar" test

Pseudomonas reactans (*P. reactans*) was streaked out in a line, directly from agar slope culture, across PAB in a Petri dish. This strain had been isolated and provided by Kinsealy Teagasc Research Centre.

The *P. tolaasii* isolate to be tested was streaked immediately after on to the plates at right angles to the reacting organism (i.e. *P. reactans*). Plates were incubated at 25°C for 24 h for the production of a white line with the reacting organism.

White line production in the agar between *P. reactans* and *P. tolaasii* was interpreted as positive interaction between colonies and a positive response for pathogenicity test.

A loopfull of pathogenicity confirmed working culture was transferred to a sterile 0.8% saline solution (Sigma, Dublin). 4 droplets of 10 µL/each of a 10^8 cfu mL^{-1} solution were inoculated onto the cap, resulting in inoculation concentration of 4×10^6 cfu.

Hyperspectral imaging

Hyperspectral images were obtained using a pushbroom line-scanning HSI instrument (DV Optics Ltd, Padua, Italy). The instrument comprised a moving table, illumination source (150 W halogen lamp source attached to a fibre optic line light positioned parallel to the moving table), mirror, objective lens (25 mm focal length), Specim V10E spectrograph (Spectral Imaging Ltd, Oulu, Finland) operating in the wavelength range of 400-1000 nm (spectroscopic resolution of 5 nm), CCD camera (Basler A312f, effective resolution of 580 × 580 pixels by 12 bits), acquisition software (SpectralScanner, DV Optics, Padua, Italy) and

PC. A cylindrical diffuser was placed in front of the fibre optic line light to produce a diffuse light source. In this study, only spectral data within the wavelength range of 445-945 nm were used, as beyond this range the noise level of the camera was high and the signal efficiency of the light source was low.

Reflectance calibration

Reflectance calibration was carried out prior to mushroom image acquisition in order to account for the background spectral response of the instrument and the "dark" camera response. The bright response ("*W*") was obtained by collecting a hypercube from a uniform white ceramic tile; the dark response ("*dark*") was acquired by turning off the light source, completely covering the lens with its cap and recording the camera response. The corrected reflectance value ("*R"*) was calculated from the measured signal ("*I"*) on a pixel-by-pixel basis as shown by:

$$R_i = \frac{(I_i - dark_i)}{(W_i - dark_i)}$$

where i is the pixel index, i.e. i=1,2,3,…,n and n is the total number of pixels.

HSI images of U mushrooms were acquired on day 0 of the experiment. MD mushrooms were scanned after 24 h of storage. PT mushroom images were taken after 48 h of storage. Data were recorded in units of reflectance and saved in ENVI header format using the acquisition software.

Confirmation of *P. tolaasii*

After image acquisition of PT mushrooms on day 2 of storage, 0.5 g of the outer skin of 10 % of each mushroom class were extracted with a sharp sterile knife. Skins were suspended separately in 10 mL of a 0.8 % saline solution. Samples were homogenised in a stomacher

168 (Seward BA 7020, Seward, UK) for 60 s at high intensity. Serial dilutions of each suspension
169 were prepared and transferred onto NA and PAB plates, which were incubated for 48 h at
170 25°C to obtain isolated colonies. The same procedure had been carried out after image
171 acquisition of U mushrooms on day 0 and resulting colonies were used as negative controls.
172 Serial dilutions of the pathogenic *P. tolaasii* solution that had been used to inoculate PT
173 mushrooms were also prepared and transferred onto NA and PAB plates; resulting colonies
174 were used as positive controls.

175 Mushroom tissue block rapid pitting and WLA tests were carried out to test for pathogenicity
176 of isolated colonies.

177 **Image processing**

178 For each mushroom hyperspectral image, 175 characteristic (i.e. U, MD or PT, depending on
179 mushroom class) regions of interest (ROI) were selected by using an interactive selection tool
180 ("*ROI tool*") available in the acquisition software. The ROI's were 3 × 3 pixels in size and
181 were selected from the central region of the mushroom cap, where possible. Selecting spectra
182 from analogous surface areas in all the mushrooms aimed at minimising the scaling
183 differences caused by mushroom surface curvature[24]. The average reflectance spectrum ("*R"*)
184 of each ROI was obtained by averaging the pixel spectra of the region. Spectral data of each
185 mushroom set were used to build two-dimensional matrices, where each row represented the
186 spectrum of one ROI.

187 Prior to the development of multivariate models for damage class prediction, spectra were
188 pre-processed using the Standard Normal Variate (SNV) transformation to reduce spectral
189 variability due to non-chemical biases[34].

190 Training set matrices (raw and SNV-corrected) contained 8400 spectra and test set matrices
191 (raw and SNV) contained 6300 spectra.

192 **Partial least squares- discriminant analysis (PLS-DA)**

193 Partial least-squares discriminant analysis was applied to the training set matrices (raw and
194 SNV-corrected, n=8400) using MATLAB 7.0 (The Math Works, Inc. USA). The aim was to
195 build models that would enable maximum separation of sample spectra into different classes
196 depending on their physical condition. A two step model approach was taken for each set of
197 spectra (i.e. raw and SNV): one model (namely "U/Dam" model) was developed to
198 discriminate between undamaged (U) and damaged (Dam) spectra and another model
199 (namely "MD/PT" model) was built to discriminate between the two classes of Dam, i.e.
200 mechanical (MD) and microbiological (PT). Overall, four models were built: U/Dam_raw,
201 U/Dam_SNV, MD/PT_raw and MD/PT_SNV.

202 For this purpose, a dummy response variable, *Y*, was constructed and assigned to each
203 spectrum. For U/Dam models, $Y = 0$ for U spectra and $Y = 1$ for Dam spectra. For MD/PT
204 models, $Y = 0$ for MD spectra and $Y = 1$ for PT spectra. In both cases, a cut-off value of 0.5
205 was used to classify spectra, as suggested by Esquerre, Gowen, O'Donnell & Downey[35];
206 spectra with a predicted dummy variable <0.5 were identified as belonging to class 0, while
207 those with predicted *Y*-value ≥0.5 were classified as belonging to class 1.

208 Spectra from the training data set were split into 10 sections and continuous blocks cross-
209 validation was performed. The decision on the number of latent variables (# LV) to select for
210 each model was made based on the root-mean square error of cross-validation (RMSECV),
211 which is the mean of the sum of squared differences between the actual and the predicted
212 value of the dummy variable.

213 The models were also applied to the test set matrices (raw and SNV-corrected, n=6300),
214 which represented independent sets of sample spectra. Performance of the classification
215 models was evaluated on the basis of their sensitivity (number of spectra of a given type

correctly classified as that type) and specificity (number of spectra not of a given type correctly classified as not of that type) on training and test sets.

Prediction maps

An important feature of hyperspectral imaging is the ability to map the distribution of components/attributes on samples. In this case, developed PLS-DA models could be applied to entire hypercubes of mushrooms to form two dimensional prediction images where the damage class of each pixel as predicted by the PLS-DA models would be represented by its intensity ("*I*"). With this in mind, the following step-by-step procedure was carried out on all mushroom hypercubes:

1. Masking. This step was performed to separate the mushroom pixels from the background. The mask was created by thresholding the mushroom image at 940 nm, where a pixel threshold value of 0.1 was used to segment the mushroom from the background. All background regions were set to zero and only the non-zero elements of the image were used in further steps.
2. Erosion. As all the spectra collected to build the models corresponded to interactively selected ROI's of the central part of the mushrooms, the image outline (i.e. edge) of the mushrooms was eroded to spectra showing differences due to sample curvature. This was done by eroding the masks using disk-shaped structuring elements (SE, whose radii increased from 0 –i.e. no erosion- to 40 pixels, in 10 pixel gaps), prior to the application of PLS-DA models. The effect that varying the radius of the SE had on i) the area of the mask, ii) the pixel distribution of the predicted maps and iii) the performance statistics of the two models at a pixel level, based upon ANOVA results obtained using R[36], was studied.

3. Application of developed PLS-DA models. The U/Dam model was applied to eroded hypercubes and following this classification, the MD/PT model was applied only to the pixels previously classified as *Dam*. Three binary images (Bin_U, Bin_{MD} and Bin_{PT}, one for each damage class, where 1 indicated class membership and 0 indicated non-membership) were generated after classifying each pixel as "*U*" ($I_{U/Dam}$<0.5), "*MD*" ($I_{U/Dam}$>0.5 and $I_{MD/PT}$<0.5) or "*PT*" ($I_{U/PT}$>0.5 and $I_{MD/PT}$>0.5) tissue.
4. Closing**.** As enzymatic browning was expected to develop uniformly across MD mushroom caps and bacterial lesions were expected to appear as brown spots of visible size, Bin_{MD} images *closed*[37] in order to avoid noise in the form of isolated *PT* pixels in such maps. The *Closing* morphological operator performs dilation followed by erosion; this was done using a diamond-shaped SE with a radius of 3 pixels. The effect of omitting/incorporating Step 4 on i) the pixel distribution of the prediction maps and ii) performance statistics, based upon ANOVA results, was investigated.
5. Concatenation: the three binary maps (i.e. Bin_U, Bin_{MD} and Bin_{PT}) were concatenated to build false colour maps where *U*, *MD* and *PT* classified pixels were represented in green, red and blue, respectively.

Mushroom classification

Based on the percentage of pixels of each damage class on the prediction map, a decision tree (shown in Figure 1) was used to allocate each mushroom to one of the three mushroom classes. As the main objective of this work was to identify *P. tolaasii* inoculated mushrooms, the *PT* pixel percentage of the prediction maps was selected as the discrimination criteria and a cut-off value was established by exploring the pixel histograms of the Bin_{PT} images of U, MD and PT mushrooms (Figure 2). A *PT* pixel percentage of 2 % appeared to be a reasonable cut-off point, as all of the U mushroom predictions and almost all of the MD mushroom predictions exhibited lower values and almost all of the PT mushroom predictions showed

higher values. After visual inspection of the two PT mushrooms that were below the cut-off value, it was observed that these two mushrooms did not develop any brown blotch on their caps, for which they could be left out for cut-off establishment purposes. As it can be seen in the figure, when the number of *PT* pixels in the prediction image was higher than 2 %, the mushroom was classified as PT. If the number of *PT* pixels was lower than 2 % and the amount of *MD* pixels was higher than the amount of *U* pixels, the mushroom was classified as MD. Finally, if the number of *PT* pixels was lower than 2 % and the amount of *MD* pixels was lower than the amount of *U* pixels, the mushroom was classified as U.

Sensitivity and specificity of the classification procedure were computed after the application of the decision tree to all of the mushroom hypercubes.

Results and discussion

RGB images

Figure 3 shows representative colour images of the three mushroom classes under investigation in this study. Mushrooms labelled as U (Figure 3a) were white in general appearance, although some of them showed some signs of natural discolouration caused by common picking and transport practice. By day one of storage, MD samples (Figure 3b) exhibited uniform browning over the entire mushroom surface. By day two of storage, *P. tolaasii* had colonised the cap of most PT mushrooms (Figure 3c), which exhibited slightly concave brown-coloured spots, the typical symptoms of brown blotch disease.

Confirmation of *P. tolaasii*

The prevalence of *Pseudomonas* in mushroom surfaces is high, but only pathogenic *P. tolaasii* is capable of causing brown blotch. Two different types of colonies, whose colours were a) creamy and b) green, were found in PAB plates of PT mushrooms, while only one type appeared in PAB plates of U mushrooms and the *P. tolaasii* inoculum; the colour of

these colonies was creamy and green, respectively. Isolates of the two types found in PT mushroom plates were obtained by re-streaking representative colonies onto fresh PAB plates. Figure 4 shows growth in PAB plates of the two types of colonies of PT mushrooms (Figures 4a, creamy colonies and 4b, green), the creamy colonies of U mushrooms (Figure 4c) and the green colonies of the *P. tolaasii* inoculum (Figure 4d). The creamy colonies of PT mushrooms (Figure 4a) were found to be similar to those found in U plates (Figure 4c), and both gave a negative response to the mushroom tissue block rapid pitting and WLA tests. The green colonies of PT mushrooms (Figure 4b) were similar to those found in *P. tolaasii* inoculum plates (Figure 4d) and both had a positive response to the two pathogenicity tests. These results confirm that the pitting observed in PT mushrooms was due to pathogenic *P. tolaasii*.

Spectra

Mean spectra of the various spectra classes are shown in Figure 5: (a) non-pretreated reflectance spectra and (b) SNV-corrected reflectance spectra. In Figure 5a, signal intensity and shape differences between U and MD spectra were remarkable. The mean MD spectrum exhibited lower reflectance values over the entire spectral region, as expected after bruising had led to loss of whiteness of the caps. The greatest differences in shape between MD and U spectra arose in the 600-800 nm region, where the mean U spectrum exhibited broader features than the mean MD spectrum. Broad spectra in the visible-near infrared wavelength range are characteristic of undamaged mushrooms, corresponding to their white appearance. The spectral differences mentioned above could be related to the formation of brown pigments, mainly melanins, which derive from enzyme-catalysed oxidation products called quinones. The mean PT spectrum appeared to be more similar in shape to the mean MD spectrum, although its slope was not as linear as MD's was in the 600-800 nm region.

Spectral differences in Figure 5a arose from differences in sample composition, but differences in illumination conditions, sample height and curvature may also have affected the spectral response of the different mushroom classes. Spectra preprocessing methods such as Multiplicative Scatter Correction (MSC)[38] and SNV[34] can be used to compensate for spectral variability caused by these external factors[39].

The mean spectra of SNV-corrected reflectance spectra of U, MD and PT spectra are shown in Figure 5b. Comparing U and MD spectra, MD exhibited higher SNV-corrected reflectance values in the 450-500 nm region and lower SNV-corrected reflectance in the 500-750 nm region. The oxidation of polyphenolic compounds and subsequent development of brown colour in the MD mushrooms might be partly responsible for this dissimilarity[35]. In the 800-950 nm region, MD spectra showed higher values than U mushrooms. Overall, the shape of the mean spectrum of PT spectra was somewhat intermediate between the mean of U and MD spectra in the wavelength range of study. The visible end of the mean PT spectrum looked more similar to MD than to U, whereas its shape in the >700 nm region was very similar to that of U mushrooms'.

PLS-DA analysis

Figure 6 shows RMSECV and performance statistics (i.e. sensitivity and specificity) of the four PLS-DA models developed, as a function of the number of latent variables (from 1 to 10). In binary classifications, the sensitivity of a model is a measure of its ability to correctly classify spectra of a given type as being of that type, whereas the specificity is a measure of its ability to correctly classify spectra which are not of a given type as not being of that type. For both U/Dam models (Figs. 6a and 6b), RMSECV exhibited a "corner" (pointed with a red dash circle) at 2 LV. The performance statistics, which were very poor at 1LV, increased at that point and remained at similar levels thereafter, for which 2 was considered to be the optimal # LV for models discriminating between U and Dam spectra. Both MD/PT models

seemed to perform best when 4 LV were selected; RMSECV did not decrease significantly after that and performance statistics remained high.

Numeric values of performance statistics of the selected models are shown in Table 1. When the models built with raw spectra were applied to the training set of spectra, almost perfect classification was achieved in the case of the U/Dam model (sensitivity = 0.997 and specificity = 1.000). The model performed worse when built on SNV-corrected spectra (sensitivity = 0.973 and specificity = 0.999); however differences in sensitivity and specificity were very small. In both cases, almost all of the Dam spectra were classified as such and none or only a few U were misclassified as Dam. When the MD/PT model was applied to the damaged spectra, the sensitivity of the raw model (sensitivity = 0.988) was higher than that of the SNV-corrected model (sensitivity = 0.963), whereas the specificity of the MD/PT_raw model was lower than the MD/PT_SNV model's (0.983 and 0.998, respectively). These results showed that almost all of the spectra of the mushrooms that had been inoculated with *P. tolaasii* were classified correctly and only a few or none of the spectra of the MD samples were misclassified as PT.

When the models were applied to the test set of spectra, the sensitivity of the U/Dam_raw model was lower (sensitivity = 0.832) but still none of the U spectra were misclassified as Dam (specificity = 1.000). Performance statistics were quite similar for the U/Dam_SNV model (sensitivity = 0.825 and specificity = 0.999). When the MD/PT model was applied to the damaged spectra of the test set, a smaller percentage of raw PT spectra were classified correctly (sensitivity = 0.661) but almost none of the MD spectra were misclassified as PT (specificity = 0.984). As observed for the previous model, the sensitivity of the MD/PT_SNV model was slightly lower (sensitivity = 0.641) and the specificity was higher (specificity = 0.998).

Overall, models built on raw reflectance spectra performed better in this study. However, with a view to generalising the use of U/Dam and MD/PT discrimination models, it might be worthwhile to compromise classification performance in favour of employing more versatile models (e.g. models built on SNV-corrected spectra).

Prediction maps

Figure 7 shows examples of prediction maps (with no erosion applied in Step 2) of (a) U, (b) MD and (c) PT mushrooms as a result of the application of raw (top row) and SNV-corrected (bottom row) PLS-DA models to the data hypercubes. Overall, predictions by models built on raw reflectance spectra appeared to be more appropriate than predictions by models built on SNV-corrected reflectance spectra: for each mushroom class, the corresponding pixel class was the main pixel class and pixels were distributed in an even manner. In the example shown (Figure 7), on the top row (i.e. predictions by models built on raw reflectance spectra), neither the map of the U mushroom nor the central region of the prediction of the MD mushroom showed misclassification, whereas most edge pixels of the latter were misclassified as U. Considering that all the spectra selected for model building belonged to central regions of the mushrooms, this misclassification could be related to the inability of the models to account for spectral differences due to mushroom surface curvature. Fewer pixels were misclassified in the prediction map of the PT mushroom, where some pixels were classified as MD. On the bottom row of Figure 7 (i.e. prediction maps by models built on SNV-corrected reflectance spectra), the maps of all mushroom types showed misclassification. For U and PT mushrooms, misclassification happened mainly but not only on the edges, where many U pixels were classified as MD. For MD mushrooms, misclassified pixels were distributed evenly along the mushroom surface. In this case, MD pixels were misclassified as PT.

385 Considering that the main focus of this work lies in the identification of PT mushrooms, after
386 visual inspection of the prediction maps (Figure 7), PLS-DA models built on non-pretreated
387 spectra were considered more appropriate for this purpose. Models built on SNV-corrected
388 reflectance spectra were therefore discarded and further sections of this paper will focus only
389 on models built on the raw data.

390 Effect of varying the radius of the SE in Step 2

391 Erosion of a binary image is a basic operation to wear the boundaries of regions away. This
392 can be done to overcome the problem introduced by the so-called "edge effect", by which
393 variability in reflection of light in introduced by spherical surfaces[40]. In this particular case,
394 where PLS-DA models were built on spectra selected from central regions of the mushrooms,
395 it was expected that these models would perform better on central areas of the mushrooms
396 than on edge regions. For this reason, masks defining the mushroom region were eroded
397 using SE's before the models were applied (see Step 2 in *Prediction maps* section). This led
398 to a decrease in misclassified pixels (typically belonging to edge regions, as observed in
399 Figure 7b, top row).

400 Figure 8a shows the effect that increasing the size of the structuring element used in this step
401 (i.e. Step 2) had on the mask (top row) and on the prediction map (bottom row) of a MD class
402 mushroom. As the radius increased (from left to right, from 0 -no erosion- to 40 pixels), the
403 mask became smaller. Consequently, the number of *MD* class pixels that were misclassified
404 (as *U* class) decreased progressively. Figure 8b shows the decrease of the average relative
405 area of the mushroom region as a function of the radius of SE, where the relative area of each
406 mask at a certain SE radius value is displayed as a percentage of the area of the mask when
407 the radius was zero (i.e. when no erosion was applied) and the average and standard deviation
408 values were obtained by considering all the mushrooms in the training and test data sets.
409 Figure 8c shows the sensitivity of the PLS-DA models built on raw reflectance spectra

applied at a pixel level as a function of the radius of the SE. The sensitivity of the U/Dam model reached its maximum (sensitivity = 1) at a radius value of 20 pixels when applied to the training set and at a radius value of 40 (sensitivity = 0.972) when applied to the test set. The sensitivity of the MD/PT model was not affected by the radius and remained at its maximum (sensitivity = 1) for the training set, whereas it increased progressively until it reached its maximum (sensitivity = 0.944) at a radius value of 40 pixels. Modifying the radius of the SE did not affect ($p>0.05$) the specificity of the PLS-DA models (results not shown).

Effect of omitting/incorporating Step 4

As the existence of isolated *PT* pixels in the prediction map had no physical meaning (brown blotch lesion on mushroom caps are detectable by the human eye), a *closing* step (see Step 4 of *Prediction maps* section) was incorporated to the prediction map routine. This step performed dilation followed by erosion on the Bin_{PT} images. Figure 9a shows how the final prediction of a MD class mushroom looked when i) Step 4 was omitted and ii) Step 4 was incorporated in the routine. As it can be observed in the figures, Step 4 removed *PT* class isolated pixels (blue) in the prediction image and converted them into pixels of class *MD* (red). The effect that such conversion had on the performance statistics of the models at a pixel level was studied and only the specificity of the MD/PT_raw model on the test set was found to change significantly ($p<0.05$). Figure 9b shows how specificity changed as the radius of the SE of Step 2 increased, when i) Step 4 was omitted (round marker) and ii) Step 4 was incorporated (square marker) in the routine. The specificity of the MD/PT_raw model improved when this step was incorporated, which means more MD class mushrooms were correctly classified. This figure suggests that adding a *closing* step was important to achieve good levels of classification.

After studying the two effects, a disk radius of 40 pixels was selected for the SE of Step 2 and it was decided to include Step 4 in the generation of prediction maps. Further sections of this paper will only focus on results based on the use of the aforementioned steps.

Mushroom classification

The application of PLS-DA models built on raw spectra to the totality of entire hypercubes led to the performance statistics shown in Table 2. For the training set mushrooms, both the sensitivity and the specificity of the U/Dam_raw model were 1, which means there was no misclassification at all. For the same samples, the sensitivity of the MD/PT_raw model was 1 and its specificity was 0.98. Only 1 out of 48 MD mushroom was misclassified as a PT mushroom. The models performed quite similarly for the mushroom hypercubes of the test set: for the U/Dam_raw model, sensitivity = 0.97 and specificity = 1. Only 2 out of 72 Dam mushrooms were misclassified as U, and none of the U was misclassified as Dam. For the MD/PT_raw model, sensitivity = 0.944 (only 2 out of 36 PT mushrooms were not classified as such) and specificity = 0.97 (only 1 MD mushroom was misclassified as being PT).

These results show the models performed well when applied at a pixel level and could be the first step towards the development of a HSI sensor that would classify independent sets of mushrooms with high levels of accuracy. Overall, the correct classification of the models presented in this paper is higher than the classification of the algorithms by Vízhányó and Felföldi[9], which correctly classified 81% of the diseased areas of test mushrooms using conventional computer imaging. It should be noted that the procedure described in this paper is longer and more complex than the one presented in that study, and the technology more costly. While the algorithms presented in the aforementioned paper discriminated diseased spots from healthy senescent mushroom parts, the models developed in this paper discriminate microbial spoilage from both undamaged and mechanically damaged samples.

458 The correct discrimination between PT and MD mushrooms ensure no misclassification of
459 samples whose colour analysis might be similar and hence avoid “false positives”.

460 Conclusion

461 Results presented in this work show that raw reflectance data of mushroom caps could be
462 used to classify mushrooms according to their damage class (i.e. undamaged, mechanically
463 damaged or brown blotch diseased). PLS-DA models were developed to initially sort
464 mushrooms into undamaged or damaged classes and to further classify the damaged into
465 mechanically damaged or microbiologically diseased classes. The application of the models
466 at a pixel level together with the use of a decision tree allowed for correct classification of
467 >95%. This study demonstrates the potential use of hyperspectral imaging as an automated
468 tool for detection of brown blotched mushrooms and for their discrimination from
469 mechanically damaged mushrooms. Knowledge gained in this research using HSI could be
470 incorporated towards the development of simpler sensors to detect and classify mushroom
471 damage of different sources. Such a system could aid the industry in increasing quality
472 control standards by correctly identifying low quality produce. However, further research and
473 validation at industrial scale are required to facilitate its adoption.

474 Acknowledgements

475 The authors would like to thank Ted Cormican and Dr. Helen Grogan from the Teagasc
476 Research Station at Kinsealy, Dublin, for producing mushrooms and providing *Pseudomonas*
477 *reactans* strains and Dr. Paula Bourke and Dr. Patricia Nobmann from Dublin Institute of
478 Technology for kind technical advice. This research was funded by the Irish Government
479 Department of Agriculture, Fisheries and Food under the Food Institutional Research
480 Measure (FIRM).

481 References

1. S.G. Paine, "Studies in Bactoeriosis II: A Brown Blotch Disease of Cultivated Mushrooms", *Annals of Applied Biology* **5,** [1919].

2. N.G. Nair and J.K. Bradley, "Mushroom Blotch Bacterium During Cultivation", *The Mushroom Journal* **90,** [1980].

3. C. Soler-Rivas, S. Jolivet, N. Arpin, J.M. Olivier and H.J. Wichers, "Biochemical and Physiological Aspects of Brown Blotch Disease of *Agaricus Bisporus*", *FEMS Microbiology Reviews* **23,** [1999].

4. P.B. Rainey, C.L. Brodey and K. Johnstone, "Biology of *Pseudomonas Tolaasii*, Cause of Brown Blotch Disease of the Cultivated Mushrooms", in *Advances in Plant Pathology* **8**, Ed by J.H. Andrews and I.C. Tommerup. Academic Press, p. 95-117 [1992].

5. F. Moquet, M. Mamoun and J.M. Olivier, "*Pseudomonas Tolaasii* and Tolaasin: Comparison of Symptom Induction on a Wide Range of *Agaricus Bisporus* Strains", *FEMS Microbiology Letters* **142,** [1996].

6. J.C. Nutkins, R.J. Mortishire-Smith, L.C. Packman, C.L. Brodey, P.B. Rainey, K. Johnstone and D.H. Williams, "Structure Determination of Tolaasin, an Extracellular Lipodepsipeptide Produced by Mushroom Pathogen *Pesudomonas Tolaasii* Paine", *Journal of American Chemical Society* **113,** [1991].

7. J.M. Olivier, J. Guillaumes and D. Martin, "Study of a Bacterial Disease of Mushroom Caps", in *4th International Conference on Plant Pathogenic Bacteria*, Angers, France [1978].

8. P.H. Heinemann, R. Hughes, C.T. Morrow, H.J. Sommer, R.B. Beelman and P.J. Wuest, "Grading of Mushrooms Using a Machine Vision System", *Transactions of the ASAE* **37,** 5 [1994].

9. T. Vízhányó and J. Felföldi, "Enhancing Colour Differences in Images of Diseased Mushrooms", *Computers and Electronics in Agriculture* **26,** [2000].

10. S. Jolivet, N. Arpin, H.J. Wichers and G. Pellom, "*Agaricus Bisporus* Browning: A Review", *Mycological Research* **102,** 12 [1998].

11. A.A. Gowen, C.P. O'Donnell, P.J. Cullen, G. Downey and J.M. Frías, "Hyperspectral Imaging - an Emerging Process Analytical Tool for Food Quality and Safety Control", *Trends in Food Science and Technology* **18,** [2007].

12. A.A. Gowen, C.P. O'Donnell, M. Taghizadeh, P.J. Cullen, J.M. Frias and G. Downey, "Characterisation of Blemishes on White Mushroom (*Agaricus Bisporus*) Caps Using Hyperspectral Imaging", in *10th International conference on Engineering and Food - ICEF 10*, Viña del Mar, Chile [2008].

13. Y. Peng and R. Lu, "Analysis of Spatially Resolved Hyperspectral Scattering Images for Assessing Apple Fruit Firmness and Soluble Solids Content", *Postharvest Biology and Technology* **48,** 1 [2008].

14. S.T. Monteiro, Y. Minekawa, Y. Kosugi, T. Akazawa and K. Oda, "Prediction of Sweetness and Amino Acid Content in Soybean Crops from Hyperspectral Imagery", *ISPRS Journal of Photogrammetry and Remote Sensing* **62,** 1 [2007].

15. J. Qiao, N. Wang, M. Ngadi and S. Baljinder, "Water Content and Weight Estimation for Potatoes Using Hyperspectral Imaging", in *2005 ASAE Annual Meeting, Paper No. 053126*, St. Joseph, Michigan, USA [2005].

16. L. Liu, M.O. Ngadi, S.O. Prasher and C. Gariépy, "Categorization of Pork Quality Using Gabor Filter-Based Hyperspectral Imaging Technology", *Journal of Food Engineering* **99,** 3 [2010].

17. H.K. Noh and R. Lu, "Hyperspectral Laser-Induced Fluorescence Imaging for Assessing Apple Fruit Quality", *Postharvest Biology and Technology* **43,** 2 [2007].

18. B. Park, K.C. Lawrence, W.R. Windham and D.P. Smith, "Performance of Hyperspectral Imaging System for Poultry Surface Fecal Contaminant Detection", *Journal of Food Engineering* **75,** 3 [2006].

19. Y. Liu, Y.-R. Chen, M.S. Kim, D.E. Chan and A.M. Lefcourt, "Development of Simple Algorithms for the Detection of Fecal Contaminants on Apples from Visible/near Infrared Hyperspectral Reflectance Imaging", *Journal of Food Engineering* **81,** 2 [2007].

20. D.P. Ariana and R. Lu, "Evaluation of Internal Defect and Surface Color of Whole Pickles Using Hyperspectral Imaging", *Journal of Food Engineering* **96,** 4 [2010].

21. J. Dubois, E. Neil Lewis, J.F.S. Fry and E.M. Calvey, "Bacterial Identification by near-Infrared Chemical Imaging of Food-Specific Cards", *Food Microbiology* **22,** 6 [2005].

22. M.F. Escoriza, J.M. VanBriesen, S. Stewart, J. Maier and P.J. Treado, "Raman Spectroscopy and Chemical Imaging for Quantification of Filtered Waterborne Bacteria", *Journal of Microbiological Methods* **66,** 1 [2006].

23. A.A. Gowen, C.P. O'Donnell, M. Taghizadeh, P.J. Cullen and G. Downey, "Hyperspectral Imaging Combined with Principal Component Analysis for Bruise Damage Detection on White Mushrooms (*Agaricus Bisporus*)", *Journal of Chemometrics* **22,** 3-4 [2008].

24. A.A. Gowen, M. Taghizadeh and C.P. O'Donnell, "Identification of Mushrooms Subjected to Freeze Damage Using Hyperspectral Imaging", *Journal of Food Engineering* **93,** 1 [2009].

25. M. Taghizadeh, A. Gowen and C.P. O'Donnell, "Prediction of White Button Mushroom (*Agaricus Bisporus*) Moisture Content Using Hyperspectral Imaging", *Sensing and Instrumentation for Food Quality and Safety* **4,** [2009].

26. E. Gaston, J.M. Frías, P.J. Cullen, C.P. O'Donnell and A.A. Gowen, "Prediction of Polyphenol Oxidase Activity Using Visible near-Infrared Hyperspectral Imaging on Mushroom (*Agaricus Bisporus*) Caps", *Journal of Agricultural and Food Chemistry*, doi: 10.1021/jf00501q.

27. M. Taghizadeh, A. Gowen and C.P. O'Donnell, "Use of Hyperspectral Imaging for Evaluation of the Shelf-Life of Fresh White Button Mushrooms (*Agaricus Bisporus*) Stored in Different Packaging Films", *Innovative Food Science and Emerging Technologies*, doi: 10.1016/j.ifset.2010.01.016.

28. A.A. Gowen, C.P. O'Donnell, M. Taghizadeh, E. Gaston, A. O'Gorman, P.J. Cullen, J.M. Frías, C. Esquerre and G. Downey, "Hyperspectral Imaging for the Investigation of Quality Deterioration in Sliced Mushrooms (*Agaricus Bisporus*) During Storage", *Sensing and Instrumentation for Food Quality and Safety* **2,** 3 [2008].

29. D.P. Ariana, R. Lu and D.E. Guyer, "Near-Infrared Hyperspectral Reflectance Imaging for Detection of Bruises on Pickling Cucumbers", *Computers and Electronics in Agriculture* **53,** 1 [2006].

30. B.M. Nicolaï, E. Lötze, A. Peirs, N. Scheerlinck and K.I. Theron, "Non-Destructive Measurement of Bitter Pit in Apple Fruit Using Nir Hyperspectral Imaging", *Postharvest Biology and Technology* **40,** 1 [2006].

31. G. ElMasry, N. Wang and C. Vigneault, "Detecting Chilling Injury in Red Delicious Apple Using Hyperspectral Imaging and Neural Networks", *Postharvest Biology and Technology* **52,** 1 [2009].

32. J. Gómez-Sanchis, L. Gómez-Chova, N. Aleixos, G. Camps-Valls, C. Montesinos-Herrero, E. Moltó and J. Blasco, "Hyperspectral System for Early Detection of Rottenness Caused by Penicillium Digitatum in Mandarins", *Journal of Food Engineering* **89,** 1 [2008].

33. W.C. Wong and T.F. Preece, "Identification of *Pseudomonas Tolaasii* : The White Line in Agar and Mushroom Tissue Block Rapid Pitting Tests", *Journal of Applied Bacteriology* **47,** [1979].

34. R.J. Barnes, M.S. Dhanoa and S.J. Lister, "Standard Normal Variate Transformation and Detrending of near Infrared Diffuse Reflectance Spectroscopy", *Applied Spectroscopy* **43,** 5 [1989].

35. C. Esquerre, A.A. Gowen, C.P. O'Donnell and G. Downey, "Initial Studies on the Quantitation of Bruise Damage and Freshness in Mushrooms Using Visible-near-Infrared Spectroscopy", *Journal of Agricultural and Food Chemistry* **57,** [2009].

36. R_Development_Core_Team, *R: A Language and Environment for Statistical Computing*. R Foundation for Statistical Computing, Vienna, Austria [2007].

37. A. Rocha, D.C. Hauagge, J. Wainer and S. Goldenstein, "Automatic Fruit and Vegetable Classification from Images", *Computers and Electronics in Agriculture* **70,** 1 [2010].

38. P. Geladi, D. MacDougall and H. Martens, "Linearization and Scatter-Correction for near-Infrared Reflectance Spectra of Meat", *Applied Spectroscopy* **39,** 3 [1985].

39. T. Azzouz, A. Puigdoménech, M. Aragay and R. Tauler, "Comparison between Different Data Pre-Treatment Methods in the Analysis of Forage Samples Using near-Infrared Diffuse Reflectance Spectroscopy and Partial Least-Squares Multivariate Calibration Method", *Analytica Chimica Acta* **484,** [2003].

40. J. Blasco, N. Aleixos and E. Moltó, "Machine Vision System for Automatic Quality Grading of Fruit", *Biosystems Engineering* **85,** 4 [2003].

606 # Figures

607 ## Figure 1

608

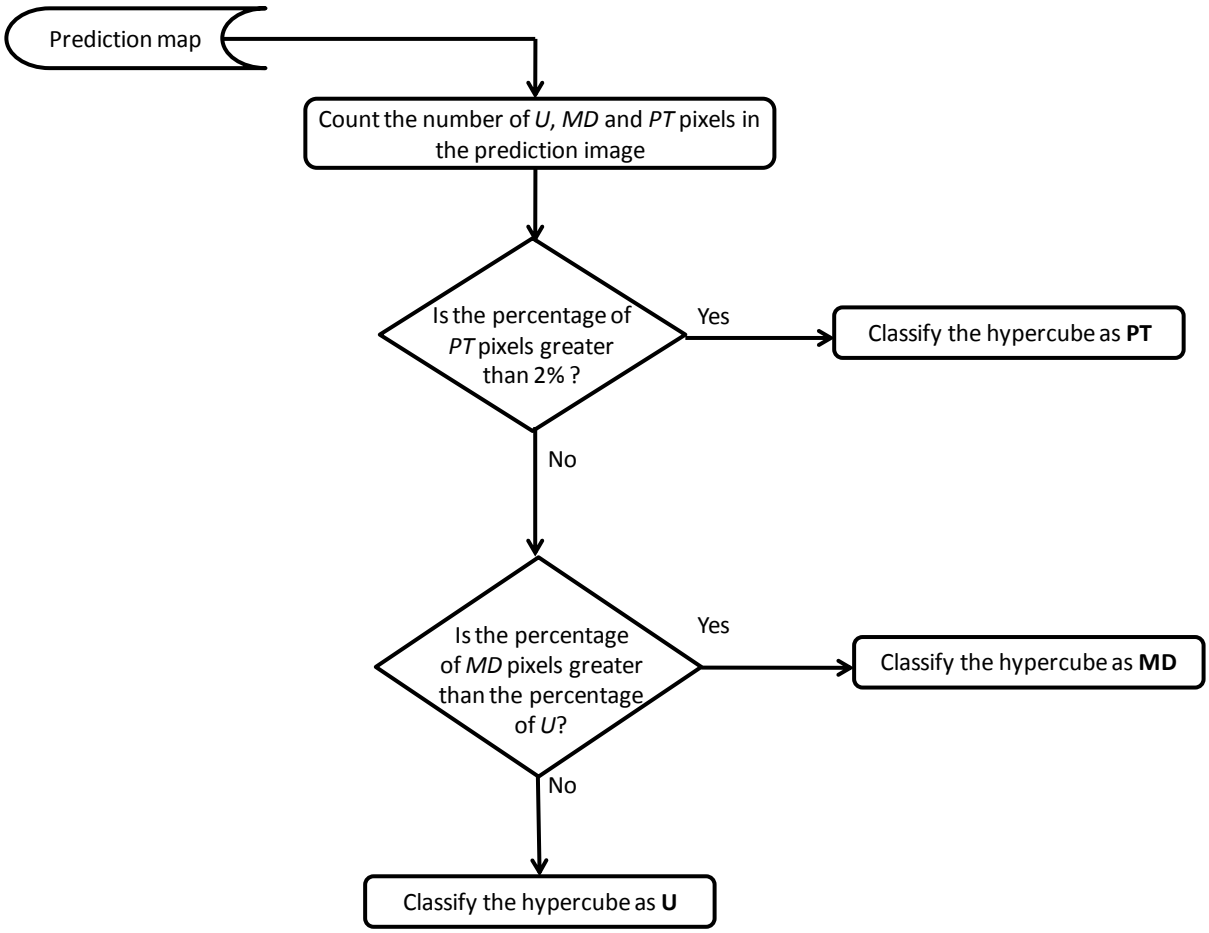

609
610

611 **Figure 1** Decision tree for mushroom hypercube classification, where U = undamaged, MD =
612 mechanically damaged and PT = P. tolaasii inoculated.

613

614

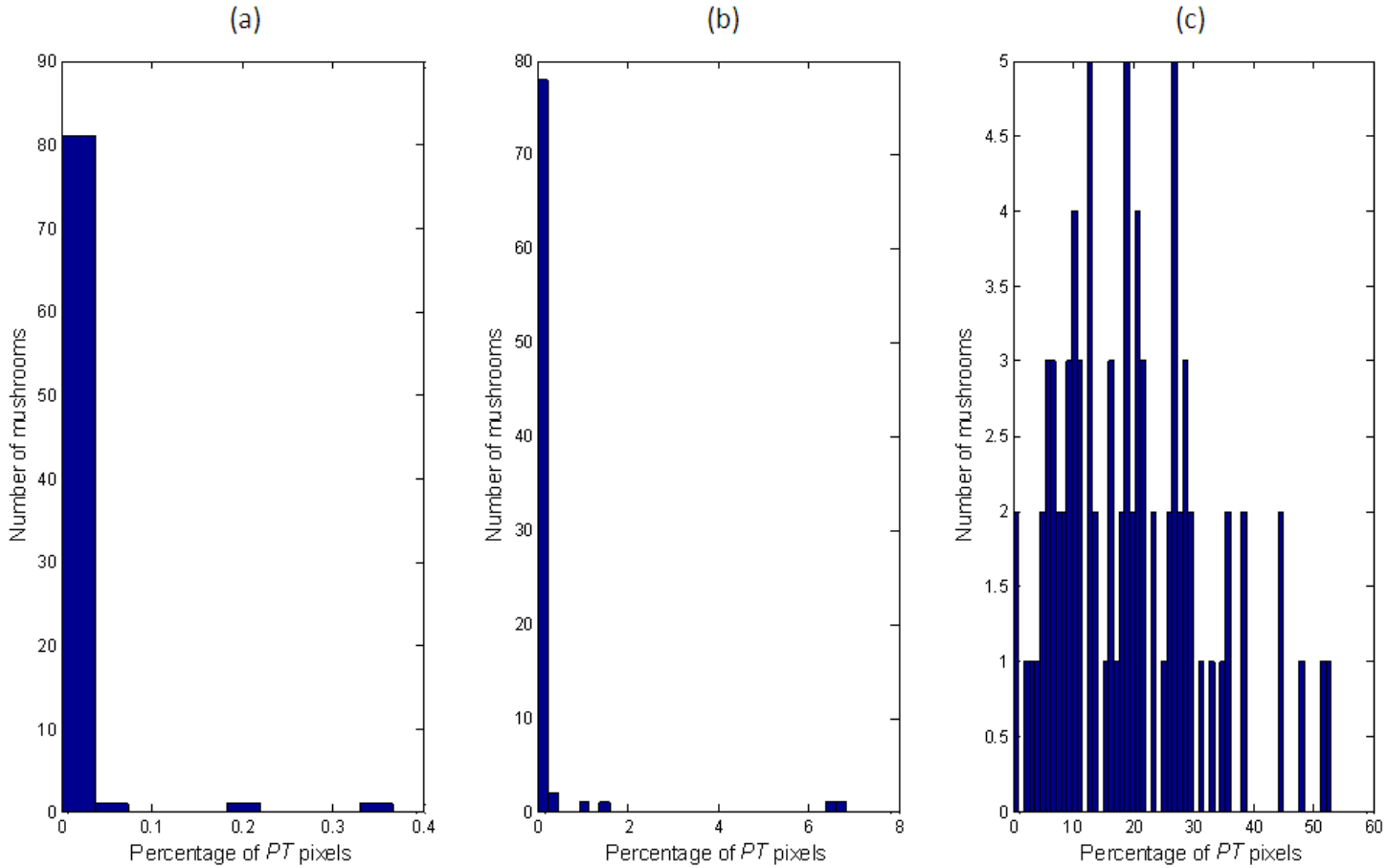

615

616 **Figure 2** Histograms showing number of mushrooms as a function of the percentage of pixels in the BIN_{PT} binary images of (a) undamaged (U),
617 (b) mechanically damaged (MD) and (c) P.tolaasii inoculated (PT) mushrooms. All the mushrooms (i.e. training and test set mushrooms) of each
618 class were plotted together, making a total of 86 samples per mushroom class.

619 **Figure 3**

620

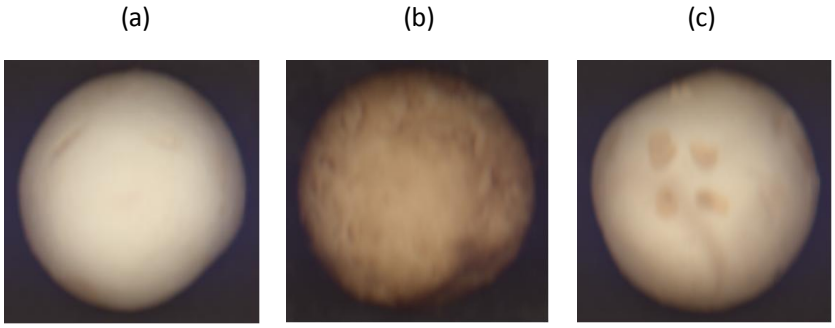

621

622 **Figure 3** Representative colour images of (a) undamaged (U), (b) mechanically damaged
623 (MD) and (c) *P. tolaasii* inoculated (PT) mushrooms.

624 **Figure 4**

625

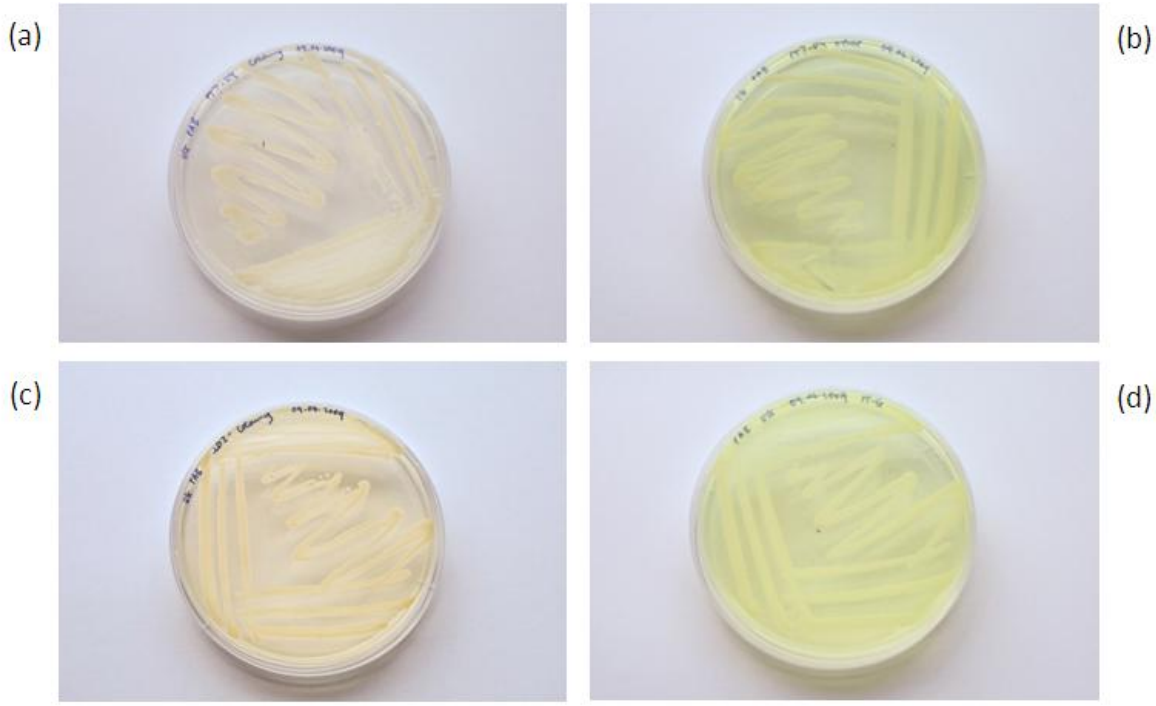

626

627 **Figure 4** (a) Creamy colonies in PAB plate of PT mushrooms, (b) Green colonies in PAB
628 plate of PT mushrooms, (c) Creamy colonies in PAB plate of U mushrooms and (d) Green
629 colonies in PAB plate of *P.tolaasii* inoculum.

630 **Figure 5**

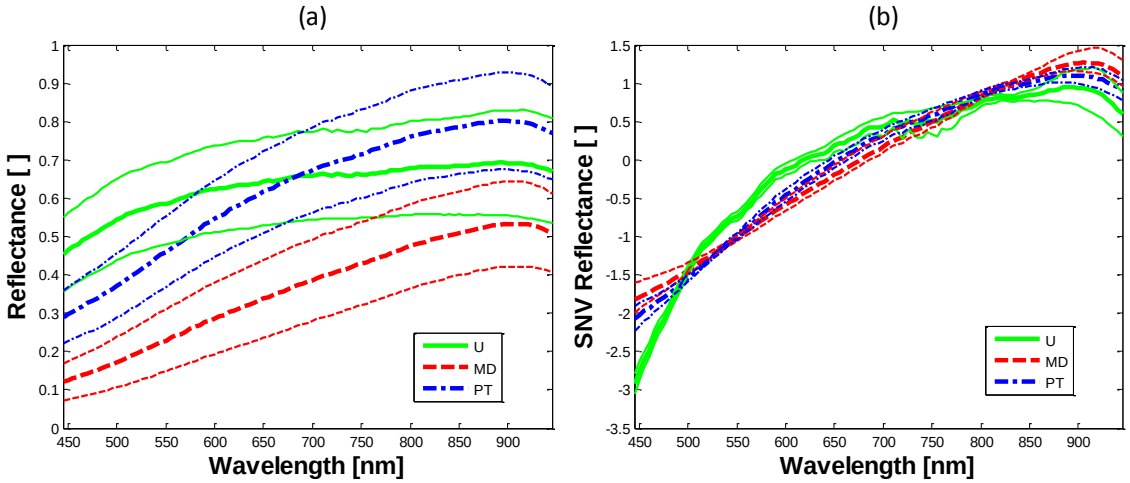

631

632 **Figure 5** (a) Mean ± standard deviation raw reflectance spectra and (b) mean ± standard
633 deviation SNV-corrected reflectance spectra of selected regions of undamaged (U),
634 mechanically damaged (MD) and *P. tolaasii* inoculated (PT) mushroom caps. For each
635 mushroom group, the broader line represents mean spectrum and the narrower lines represent
636 ± standard deviation spectra.
637

638 **Figure 6**

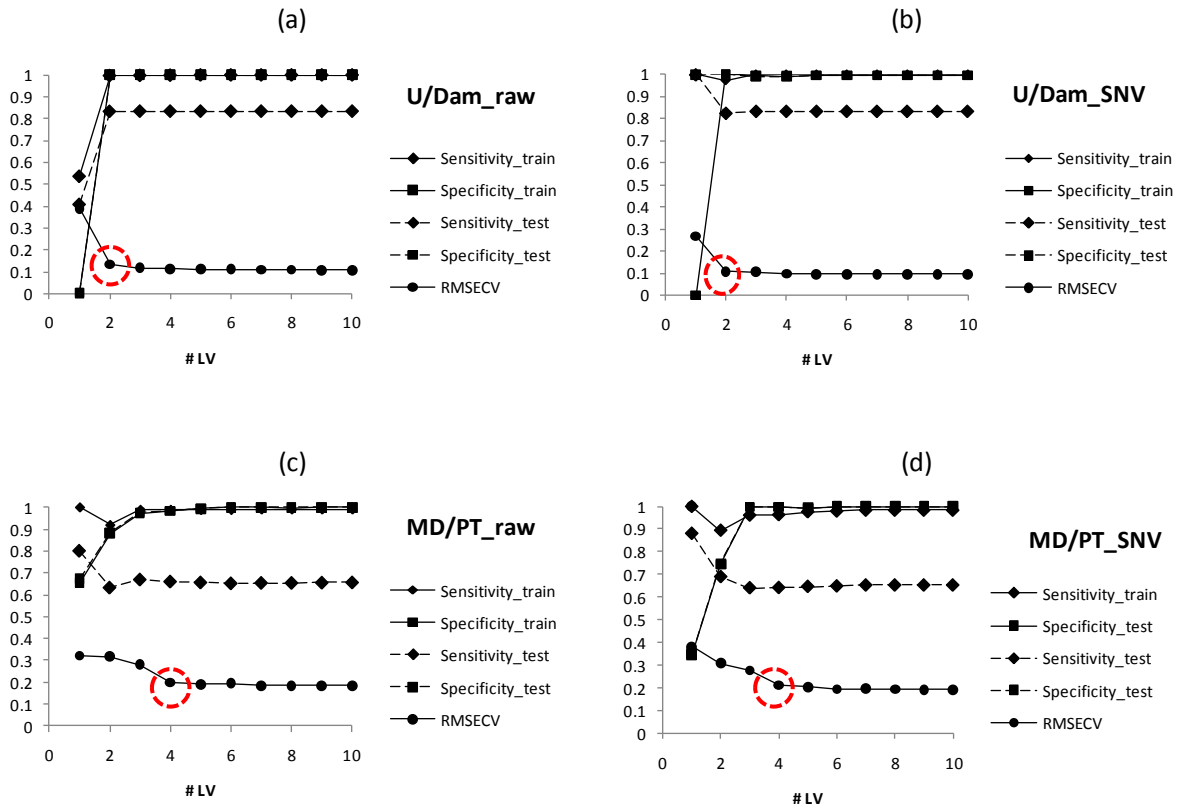

639

640 **Figure 6** Root-mean square error of cross-validation (RMSECV) and performance statistics
641 (i.e. sensitivity and specificity) of PLS-DA models of (a) U/Dam_raw model, (b)
642 U/Dam_SNV model, (c) MD/PT_raw model and (d) MD/PT_SNV model as a function of the
643 number of latent variables (# LV), where _train = training set and _test = test set.

644 **Figure 7**

645

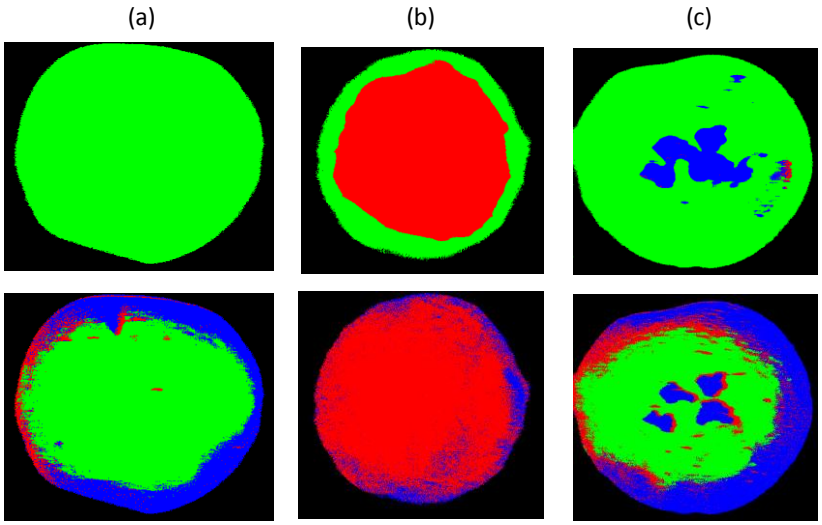

646

647 **Figure 7** Prediction images (after no erosion in Step 2) of (a) undamaged (U), (b)
648 mechanically damaged (MD) and (c) *P. tolaasii* inoculated (PT) mushrooms by PLS-DA
649 models built on raw reflectance spectra (top row) and SNV-corrected reflectance spectra
650 (bottom row).

651 **Figure 8**

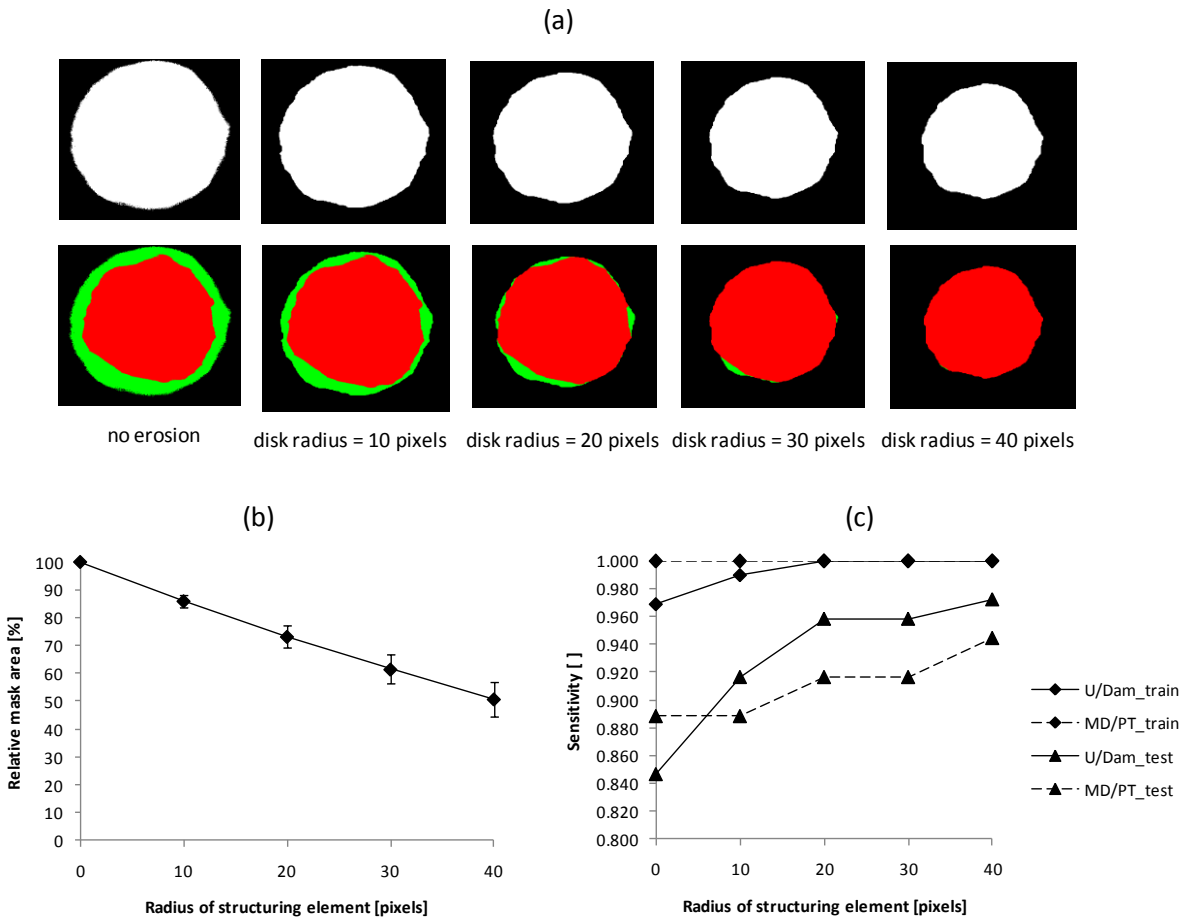

652

653 **Figure 8** (a) Binary masks (top row) and prediction maps (bottom row) of a mechanically
654 damaged (MD) mushroom, (b) Average relative mask area ± SD and (c) Sensitivity of PLS-
655 DA models, as a function of the radius of the structuring element (SE) used for erosion in
656 Step 2.

657 **Figure 9**

658

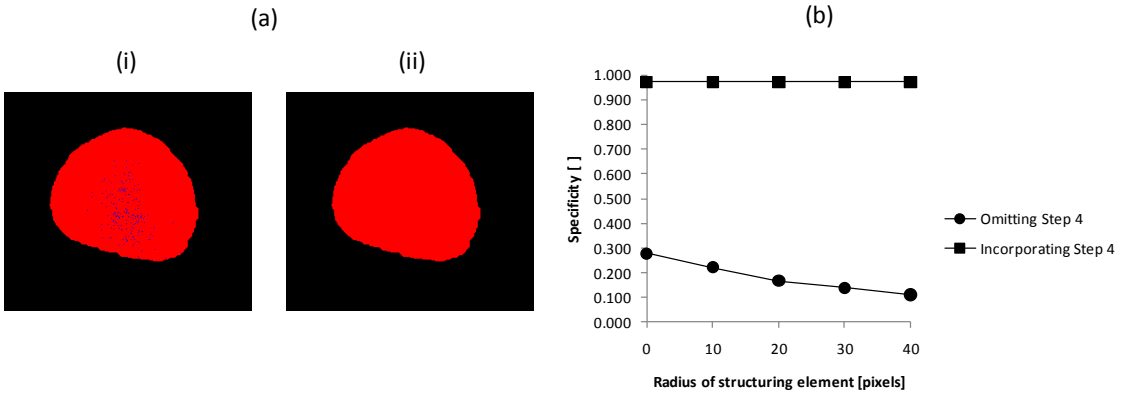

659

660 **Figure 9** Effect of the exclusion/incorporation of Step 4 to the prediction map routine in
661 terms of (a) the pixel distribution in the prediction map of a mechanically damaged (MD)
662 mushroom when (i) Step 4 was omitted and (ii) Step 4 was incorporated and (b) the
663 Specificity of the MD/PT_raw model on the test set as a function of the radius of the
664 structuring element (SE) used for erosion in Step 2.

665 .

Tables

Table 1

Table 1 Performance statistics at spectra level of all the PLS-DA models built on reflectance spectra.

		TRAINING SET		TEST SET	
Model	**# LV**	**Sensitivity**	**Specificity**	**Sensitivity**	**Specificity**
U/Dam_raw	2	0.997	1	0.832	1
U/Dam_SNV	2	0.973	0.999	0.825	0.999
MD/PT_raw	4	0.988	0.983	0.661	0.984
MD/PT_SNV	4	0.963	0.998	0.641	0.998

671 **Table 2**

672 **Table 2** Performance statistics at a pixel level PLS-DA models built on raw reflectance
673 spectra.

	TRAINING SET		TEST SET	
Model	**Sensitivity**	**Specificity**	**Sensitivity**	**Specificity**
U/Dam_raw	1	1	0.972	1
MD/PT_raw	1	0.979	0.944	0.972

674